ELSEVIER

Journal of Nuclear Materials 281 (2000) 57–64

journal of nuclear materials

www.elsevier.nl/locate/jnucmat

Ultra-high vacuum investigation of the surface chemistry of zirconium

Y.C. Kang, M.M. Milovancev, D.A. Clauss, M.A. Lange, R.D. Ramsier *

Department of Physics, Buchtel College of Arts and Sciences, University of Akron, Akron, OH 44325-4001, USA

Received 27 March 2000; accepted 8 May 2000

Abstract

A description of a new ultra-high vacuum chamber for studying zirconium surface chemistry is presented. The design includes low-energy electron diffraction (LEED) and scanning tunneling microscopy, a gas-handling system for controlled gas exposure, a mass spectrometer for temperature programmed desorption (TPD), an electron gun for electronically inducing surface chemistry, and Auger electron spectroscopy (AES). Schematic representations of the apparatus are described, followed by the first application of TPD and LEED in this system to water adsorption on Zr(0 0 0 1). Water adsorption at 180 K followed by linear heating results in water desorption in a broad TPD feature near 550 K. Data from LEED indicate that this adsorption does not result in ordered layers until 700 K annealing, and that formation of ordered structures depends on exposure and annealing conditions. These TPD and LEED data indicate a competition between the kinetics of recombination and desorption with those of diffusion involving the subsurface regions.

PACS: 82.65; 68.10

1. Introduction

The properties and surface reactivity of zirconium have been extensively studied in the scientific literature. Zirconium is very reactive chemically in its pure form especially with respect to light elements, however the formation of a tough, protective oxide layer on its surface is believed to be responsible for its excellent corrosion resistance in many adverse environments. Compared to other metals, zirconium exhibits a high melting point, good thermal conductivity, low thermal expansion, acceptable strength, and is strongly heat and pressure resistant. It also has a very low neutron scattering cross-section and a high solid solubility of oxygen and hydrogen. Due to its corrosion resistance, zirconium and its alloys are increasingly being used in applications for pollution control and chemical processing equipment, acid manufacturing, oceanic instruments, marine hardware, and pump and valve sets [1]. In addition to its corrosion resistance, its low neutron scattering cross-section has made it the material of choice for fuel containment in water-cooled nuclear reactors [2,3]. Stress corrosion cracking (SCC) of zirconium metals and alloys when utilized in adverse chemical and nuclear reactor conditions has been summarized by Yau [4].

Surface science studies of polycrystalline zirconium relevant to this work [5–8] have utilized techniques such as Auger electron spectroscopy (AES) [5–7], temperature programmed desorption (TPD) [5,8], and electron stimulated desorption (ESD) [8]. Diffusion coefficients for surface to bulk transport have been determined for C, O, and N adsorbed on polycrystalline zirconium by monitoring AES signals to determine surface composition over time [5]. In the same study, dissociation products were found to preferentially diffuse into the metal upon heating of the substrate instead of desorbing, and it was determined that nitrogen forms an underlayer within zirconium. Another study of polycrystalline zirconium indicates that the passive oxide layer that forms on the surface resists subsequent

* Corresponding author. Tel.: +1-330 972 4936; fax: +1-330 972 6918.

E-mail address: rex@uakron.edu (R.D. Ramsier).

0022-3115/00/$ - see front matter
PII: S0022-3115(00)00131-8

adsorption of hydrogen but attracts hydrogen from within the bulk to the surface [8]. Oxidation of polycrystalline zirconium and Zircaloy-2 studied via chemisorption of oxygen and water vapor, demonstrated the formation of suboxides (Zr_2O, ZrO, Zr_2O_3) along with the primary oxide ZrO_2 [7].

The Zr(0 0 0 1) surface has also been the subject of recent investigation [9–23]. The kinetics of surface oxidation have been studied on the basal plane [11] on which oxide layer growth occurs layer by layer at 90 and 293 K and by island formation after the first two monolayers (ML) at 293 K. In a related study, low coverages (0–0.5 ML) of oxygen on Zr(0 0 0 1) were examined at 90, 293, and 473 K and results indicate that much of the oxygen adsorbs in subsurface sites that limit further diffusion of oxygen into the bulk [12]. Tensor low-energy electron diffraction (LEED) studies of 0.5 and 1.0 ML coverages of oxygen on Zr(0 0 0 1) [13,14] show that oxygen resides in the octahedral holes within the first three Zr layers. Another tensor LEED study of 2.0 ML coverage of oxygen on Zr(0 0 0 1) indicates that oxygen resides in tetrahedral hole sites inside the first layer of zirconium atoms and as an overlayer in vacant sites on the surface [15].

The diffusion of oxygen along the *c* axis of Zr(0 0 0 1) has been determined by AES analysis and described by kinetic models [9,20]. A continuum model was initially utilized in these studies [9] and later replaced by a discrete hopping model that could account for differences between surface and bulk ad(ab)sorption sites for oxygen atoms [20]. The effect of the surface region on the dissolution of oxygen into zirconium was found to be minimal in this study, however the authors caution the use of their model under high coverage conditions, where inter-adsorbate interactions may become important.

The behavior of hydrogen adsorbed on Zr(0 0 0 1) is also complex [21–23]. The surface concentration of hydrogen depends on the gas exposure as well as on the annealing history of the sample. High temperature annealing (up to 923 K) removed the surface hydrogen but no desorption was detected, indicating that hydrogen diffused into the bulk [21]. Further annealing studies [22,23] of samples with known bulk concentrations of hydrogen indicate that there is a critical temperature below which hydrogen segregates to the Zr(0 0 0 1) surface and forms a hydride-like phase. The presence of oxygen in the near surface region was found to increase the rate of hydrogen segregation to the surface below the critical temperature [23].

The adsorption of D_2O on Zr(0 0 0 1) at 80 K has been studied using TPD and other techniques [10]. Under these conditions, water adsorbs in three reasonably distinct stages: a low coverage dissociatively adsorbed layer, a molecularly adsorbed second layer at higher coverages and a subsequent ice layer at the highest coverages. The ice layer desorbs at 163 K and most (80–90%) of the second layer desorbs at 175 K during TPD. The species remaining from the first and second layer form a temperature dependent mixture of adsorbed O, D, and OD, and unexpected D_2 desorption was observed above 300 K. Finally, exposure of Zr(0 0 0 1) to D_2O at temperatures in the range 200–273 K results in the release of D_2 gas and the formation of adsorbed oxygen islands on the surface [19]. The rate of water decomposition in this temperature range was found to be a weak function of temperature but a strong function of oxygen coverage. At temperatures outside of this range, the kinetic model based on oxygen island formation does not adequately describe the experimental results.

In the present study, a newly constructed ultra-high vacuum system is applied for the first time to the investigation of the chemical reactivity of zirconium surfaces. Deuterium oxide adsorption at 180 K and subsequent reaction on Zr(0 0 0 1) is monitored by LEED and TPD. Isotopic water is used in an attempt to distinguish the role of hydrogen within the Zr crystal from that of the dissociation products of water on the surface. This study is the first in a planned series of efforts aimed at understanding the reactivity of small molecules on zirconium surfaces including the role of bulk and subsurface species in the presence of thermal and electronic excitation.

2. Experimental apparatus and procedure

In this section, a description of a new vacuum chamber designed for controlled studies of zirconium surface chemistry is presented. Although all of the features of the new system are not utilized in the present study, schematic representations and general principles of operation are explained to serve as a reference for future work. The base pressure attained in the chamber described herein is 1.5×10^{-8} Pa as read with a nude ion gauge that has not been corrected for ionization probability.

The pumping systems can be separated into two primary groups. The first set of pumps includes a water-cooled 360 l/s turbomolecular pump (TMP) backed by a dual stage oil sealed rotary vane roughing pump (RP). The TMP/RP combination, depicted in Fig. 1 as part of the entire vacuum chamber, are separated from the bulk of the chamber by the main gate valve. These pumps are primarily used to exhaust the chamber during bakeout, to purge argon introduced into the chamber during argon sputter cleaning, and to evacuate the chamber from atmospheric pressure to high vacuum. Once bakeout is complete, these pumps are generally used to pump the attached gas handling system and the load-locked sample preparation chamber.

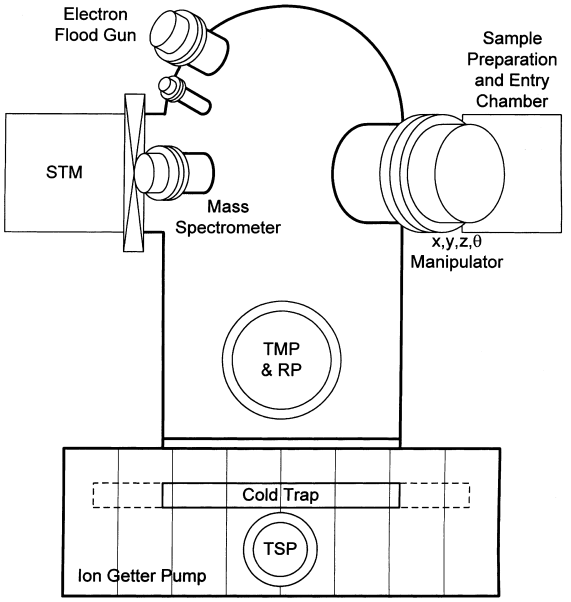

Fig. 1. Schematic representation (front view) of the new ultra-high vacuum system.

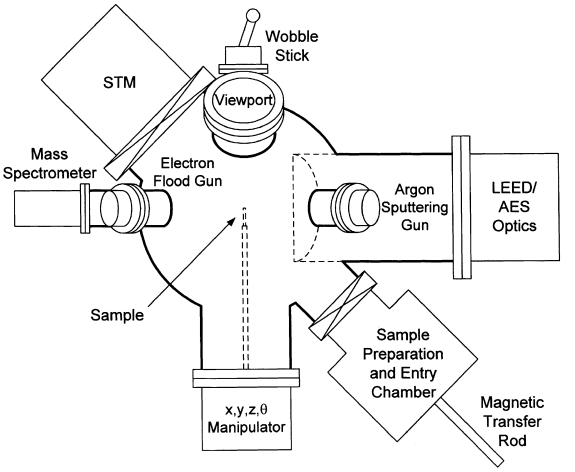

Fig. 2. Schematic representation (top view) of the new ultra-high vacuum system.

The second set of pumps displayed in Fig. 1 includes a four-filament titanium sublimation pump (TSP), a toroidal ion getter pump and a liquid-nitrogen-cooled cold trap. This set of pumps can be isolated from the rest of the vacuum chamber by a horizontal poppet valve (not shown). Three nude ion gauges are placed so as to measure the pressure in different regions of the system. The quadrupole mass spectrometer (QMS) also displays a local total pressure as do the capacitance manometers (CM) located on the gas handling system.

Attached to the main system via another gate valve is a preparation chamber as shown in Fig. 2. The preparation chamber contains a thermal evaporation source as well as a DC planar magnetron sputtering source, a film thickness/rate monitor, and an ion gauge. A magnetically coupled sample transfer rod, also depicted in Fig. 2, is mounted on the exterior end of the preparation chamber. It allows samples to be moved between the preparation chamber and the main chamber, as well as through to the isolated UHV-compatible scanning tunneling microscope (STM).

A stainless steel gas handling system incorporating two precision variable leak valves is depicted in Fig. 3. The custom-made system allows for controlled, reproducible and independent introduction of both inert and reactive gases into either the main chamber or the preparation chamber. The main chamber can either be backfilled with the gas of interest, or the sample can be dosed in a line-of-sight fashion with a molecular beam doser (not presently installed). The gas line itself has two isolatable regions. One half of the system allows the introduction of reactive gases and is monitored by a 1.33×10^3 Pa CM as shown in Fig. 3 (CM 1), while the other half of the gas line is for inert gas control and contains a 1.33×10^5 Pa CM (CM 2).

An argon ion gun is located on the main chamber for sample surface cleaning and opposite this an electron

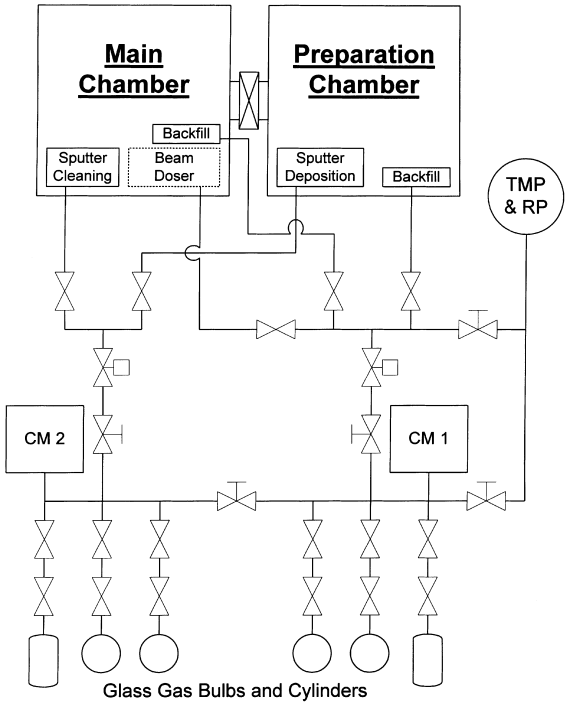

Fig. 3. Schematic representation of the new gas handling system.

flood gun is positioned for bombarding species chemisorbed on the sample for controlled studies of electron-stimulated surface processes. A reverse-view, retractable four-grid LEED system is combined with a retarding field AES so that they utilize a single vacuum flange on the main chamber. A video camera is used to record the back-scattered electron diffraction patterns appearing on a phosphor screen through a viewport.

The vacuum chamber is also equipped with a manipulator that allows limited sample motion along three orthogonal axes and provides rotational capability about the manipulator axis. The manipulator, denoted as the x, y, z, θ manipulator in Figs. 1 and 2, allows samples mounted on the manipulator arm to be cooled by liquid nitrogen as well as resistively heated and controlled by a temperature controller. The sides of the substrate are spot-welded to tantalum wires, which are in turn mounted onto machined copper arms. A copper braid connects a cold finger to one of the copper arms to provide cooling of the sample. Insulated wires are connected to the copper arms of the manipulator chassis for sample heating. The sample is electrically isolated from the manipulator arm by sapphire. Two type-E thermocouples are directly spot-welded onto the sides of the sample to monitor sample temperature. A small phosphor screen is installed on the side of the manipulator arm opposite to the polished face of the sample and is used to focus the electron guns.

The single crystal Zr(0 0 0 1) sample was prepared by Mateck Material-Technologie & Kristalle, and is in the form of a cylindrical disk (diameter 6 mm and thickness 1 mm). One side of the sample is polished to a surface roughness of 0.03 μm and the uncertainty in orientation of the sample is less than 1 degree. Once the vacuum system bakeout is complete, the sample is cleaned by Ar^+ sputtering (2 keV, 2×10^4 μA/m^2) in 2 h cycles with the sample at 180 K followed by annealing to 840 K for 2 min after each cleaning cycle. LEED patterns were observed and collected using a video camera and an image grabber intermittently throughout the initial sputter cleaning of the sample. The LEED images (60–70 eV, 2×10^4 μA/m^2) improved after each argon sputter cycle and exhibited sharp (1×1) patterns characteristic of the Zr(0 0 0 1) sample before experiments were performed.

Liquid deuterium oxide (D_2O, 99.5% purity) was placed into a glass bulb fitted with a Kovar seal joint that mounts directly to a stainless steel bellows valve. The glass bulb was then connected to the reactive-gas portion of the stainless steel gas handling system. An argon (99.9999% purity) cylinder is connected to the inert portion of the gas line for sample cleaning. Contamination of gases on the gas line is kept to a minimum by complete system bakeout, separate bakeout of the gas handling system, and repetitive freeze-pump-thaw cycles as appropriate. Gases are backfilled into the main vacuum system through the precision leak valves and exposures within the chamber as measured by the QMS are reported in Langmuir (L) units ($1\ L = 1.33 \times 10^{-4}$ Pa s). The relative abundance of the residual gases within the chamber as well as during gas dosing was measured using the QMS to rule out the possibility of contamination.

3. Overview of temperature programmed desorption

Temperature programmed desorption, also known as thermal desorption spectroscopy (TDS), is a powerful technique used to study desorption in a controlled manner [24–26]. In TPD, a clean surface is exposed to a low pressure of a known gas under UHV conditions. Some of the gas may chemisorb or physisorb to a variety of surfaces within the vacuum chamber, and the remainder is pumped away. In equilibrium, this adsorbed gas will remain bound to the surfaces until it is externally influenced either thermally or electronically.

The sample mounted onto the manipulator described in Section 2 is continuously cooled throughout the process thus increasing the sticking probability of the gas to the surface of interest. The temperature controller in a regulated fashion then resistively heats the sample and species desorb from the surface at a rate governed by the Boltzmann factor. The desorbing species are monitored by the QMS and the data yield information on the nature of adsorbate–substrate bonding and surface reactions. Temperatures where desorption rates is substantial appear as peaks in TPD spectra of desorption rates versus temperature. The sample is positioned directly in front of the QMS to increase the probability that all detected species originate from the sample and not from other surfaces in the vacuum chamber.

The thermal desorption rate of particles from a sample surface may be described by

$$R_d = -(dN/dt) = (v)^{\alpha}(N)^{\alpha} \exp(-E_d/kT), \quad (1)$$

where R_d is the desorption rate, E_d the apparent activation energy of desorption, N the number of adsorbed species on the sample surface, T the absolute temperature of the sample, v the pre-exponential factor of desorption, α the desorption order, and k is Boltzmann's constant. The height of the desorption features in TPD spectra is proportional to the rate of desorption and the integrated area is proportional to the number of species that desorb from the surface. In analyzing experimental TPD spectra, it is often possible to determine important information such as the number and identity of particles that desorb, the apparent activation energy of

desorption, the pre-exponential factor of desorption, and the desorption order.

The actual physical description of the pre-exponential factor of desorption has been argued by many authors. The factor v has the dimensions of frequency (inverse time) and is usually assumed to be 10^{13} s^{-1}. This approach assumes that the factor v is related to the frequency of vibration of an adsorbate on a substrate surface. The pre-exponential factor has also been discussed as an entropy-related term associated with the amount of possible configurations of the gas–solid system. In the case of zirconium, where it is known that diffusion into and out of the bulk and near surface regions competes with desorption [27,28], TPD analysis and interpretation of kinetic parameters is expected to be complex.

4. Results and discussion

The QMS, in multiple ion acquisition mode, was set to measure the partial pressure of H_2O (18 amu), HDO (19 amu), and D_2O (20 amu). The 18 amu signal from normal water (H_2O^+) also contains signal from heavy water (OD^+), and this is accounted for before the 18 amu signal is used as a measure of the presence of H_2O. Although high purity D_2O was utilized during dosing in all experiments, hydrogen exchange in the storage bulb and dosing line occurs, and the reactivity of Zr mandates that the presence of residual H_2O in the vacuum system also be accounted for in determining water exposures. The QMS monitored the partial pressures of these three species throughout the backfilling process, and sample exposures (in Langmuir units) are calculated from the sum of the integrated areas of these dosing curves.

Fig. 4 presents representative TPD spectra of D_2O following various exposures to isotopic water by backfilling at 180 K. This adsorption temperature is just high enough to avoid the molecularly chemisorbed and physisorbed layers identified by Li et al. [10], and is in the range where another paper by Li et al. [19] reported the kinetics of water adsorption to be complicated. The data of Fig. 4 indicate that the desorption of water in the present situation is also complex. At low exposures, essentially no desorption feature is apparent, and as the exposure increases a feature with a shoulder grows and shifts to higher temperature. The desorption yield is not rigorously monotonic with exposure, nor is the desorption peak profile. This would seem to indicate that there is a memory effect, where the desorption kinetics depend on the annealing and adsorption history of the substrate. In order to compensate for this possibility, data were collected in random order (with respect to exposure) and over a

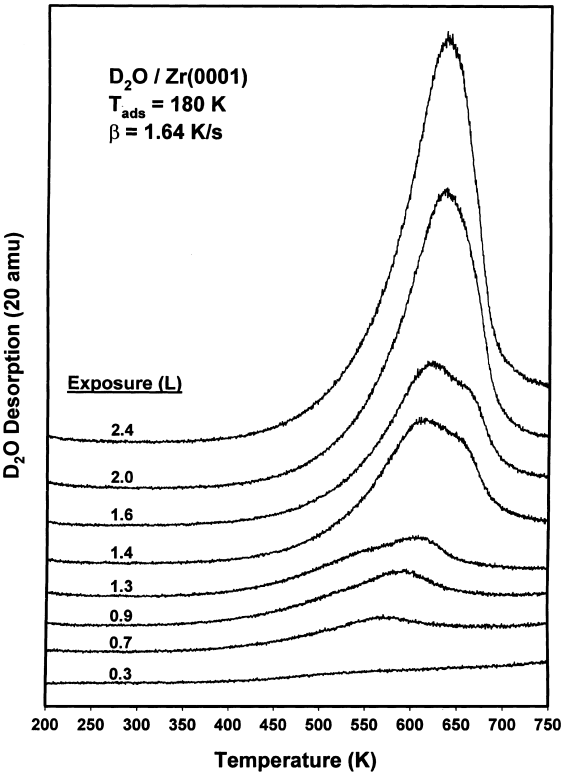

Fig. 4. Representative TPD spectra of deuterium oxide from Zr(0 0 0 1) following 180 K adsorption of isotopic water at various exposures.

period of several days, with sputtering/annealing cycles performed on each day.

The possibility of artifacts due to spurious heating effects in data such as these has been investigated by using different sample heating assemblies and sample geometries, however behavior similar to that in Fig. 4 is always observed. The ratio of the integrated areas of the D_2O desorption features to those of HDO and H_2O are approximately 4:2:1 for the data of Fig. 4, essentially identical to the same ratios measured in the dosing gas within experimental uncertainty. The desorption peak profiles of HDO and H_2O (not shown) are the same as D_2O for any given experimental run, thus we are unable to identify any isotope-selective desorption kinetics in this study. However, we have identified experimental conditions where recombinative water desorption occurs from Zr(0 0 0 1) in the temperature range 550–650 K, and the lack of isotopic selectivity may indicate that this desorption originates from surface and subsurface species but not from diffusion into/out of the bulk.

The data of Fig. 5 represent the integrated TPD yield of D_2O versus total water exposure taken from the data of Fig. 4 and similar TPD runs. The uncertainty bars result from fitting a baseline to the mass-selective QMS

data in order to numerically calculate the exposures and TPD yields. It can be seen in Fig. 5 that the TPD yield increases with 180 K water exposure; however the large uncertainties in these data make polynomial fits unreliable. Although the recombinative desorption of water observed in this study occurs in the temperature range where nuclear reaction analysis and work function measurements indicate that the surface coverage of adsorbates is changing [10], this may be coincidental. This previous work [10] utilized an adsorption temperature of 80 K, and the sticking coefficient and reactivity of water on this surface is known to strongly depend on adsorption temperature [19]. In fact, desorption of molecular oxygen or hydrogen (deuterium) was not observed in any TPD experiments under the present experimental conditions, but unexpected D_2 desorption was detected near 325 K in Ref. [10] at exposures high enough to begin filling the second adsorbed layer. Unexpected behavior in TPD studies of polycrystalline Zr is also reported in [8], where exposure to O_2 at 300 K results in the thermal desorption of H_2 near 500 K.

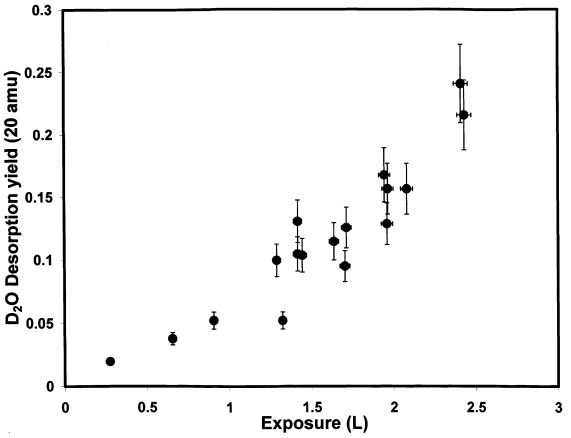

Fig. 5. Total TPD yield (arbitrary units) of deuterium oxide from Zr(0 0 0 1) as determined from the integrated areas of spectra such as those in Fig. 4.

The LEED data collected in this study (a representative set is presented in Fig. 6) indicate that the adsorption of water on Zr(0 0 0 1) at 180 K does not result in ordered overlayer structures but does produce an increase in the diffuse background in LEED patterns (Fig. 6(B)). Annealing to 400 K reduces this background intensity (Fig. 6(C)), probably indicating adsorbate

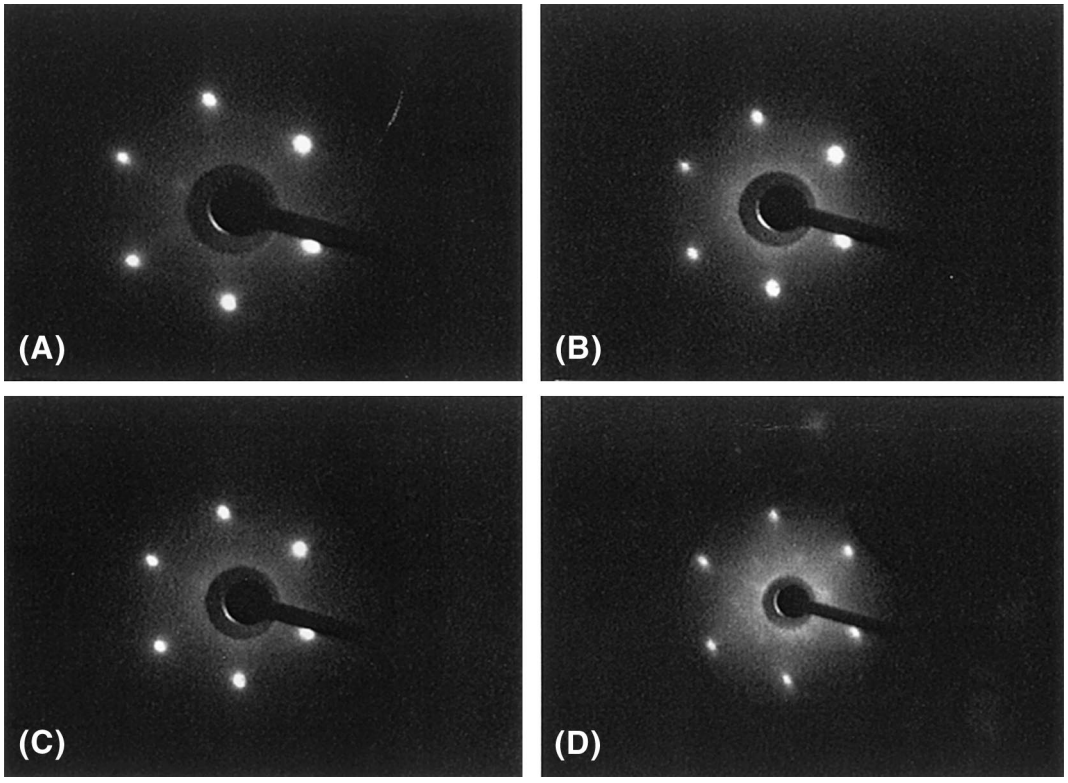

Fig. 6. Representative LEED data from Zr(0 0 0 1) subjected to isotopic water adsorption and annealing: (A) clean Zr(0 0 0 1) surface; (B) after dosing D_2O (1.4 L); (C) after heating to 400 K; (D) after heating to 700 K.

dissolution into the substrate. Only after annealing to 700 K are there faint yet distinct LEED features corresponding to the adsorbed layers (Fig. 6(D)). Analysis indicates a $(\sqrt{3} \times \sqrt{3})$R30° pattern, and streaking that may indicate the presence of a (2×2) pattern. These results are similar to those observed for high D_2O coverages on Zr(0 0 0 1) at 80 K followed by 623 K annealing [10], and is believed to result from the presence of oxygen. No ordered structures have been identified over a wide range of exposures in this study unless annealing is performed, and the formation of distinct LEED patterns due to overlayer structures is dependent on the exposure, annealing temperature, and substrate history.

The data collected in this study, in conjunction with the limited amount of related literature presently available [8,10,19], point to a strong coupling between the presence of hydrogenic and oxygenic species and the adsorption temperature in determining the resulting desorption kinetics from Zr surfaces. It is probable that the formation of subsurface adsorbate layers occurs via temperature-dependent dissolution, as evidenced by the LEED data and inferred by the complicated TPD peak profiles and temperature shifts. The diffusion of only one species into and out of the substrate during temperature ramping is sufficient to rule out the application of simple models such as Eq. (1) for modeling the presented TPD data [27,28]. However, the interaction between O and H species in the coadsorbed state may drive effective rate constants and diffusion coefficients far from those seen in either adsorption system independently. It is clear from this initial study performed in this laboratory that the surface chemistry of zirconium is complex, and that further investigation is necessary in order to develop a more complete understanding of this materials system.

5. Conclusions

This study presents a schematic description of a new surface analysis system designed for well-controlled studies of the surface chemistry of zirconium in the presence of small adsorbed molecules. The initial application of this system utilizing TPD and LEED indicates that the kinetics of desorption of water from Zr(0 0 0 1) depends not only on the water exposure, but also probably on the exposure/annealing history of the surface. The data are interpreted as resulting from a competition between the kinetics of desorption from and diffusion into/out of the substrate, complicated by the influence of oxygen on the kinetics of hydrogen and vice versa. No preferential isotopic mixing was identified that would indicate a dominant kinetic mechanism, however this may indicate that the recombinative desorption observed originates from the surface and near-surface regions and not from the bulk. Further investigation and modeling is warranted by the results presented herein.

Acknowledgements

Support of this work by Fermenthaus Canada, The Aluminum Corporation of America, and The Office of Research Services and Sponsored Programs at the University of Akron is greatly appreciated.

References

[1] T.-L. Yau, B.O. Paul, R.H. Henson, Chem. Process. 62 (1999) 70.
[2] P. Cohen, Water Coolant Technology of Power Reactors, American Nuclear Society, USA, 1980.
[3] D. Bodansky, Nuclear Energy: Principles, Practices and Prospects, AIP, New York, 1996.
[4] T.-L. Yau, in: R.H. Jones (Ed.), Stress-Corrosion Cracking, ASM International, Materials Park, 1992 (Chapter 11).
[5] J.S. Foord, P.J. Goddard, R.M. Lambert, Surf. Sci. 94 (1980) 339.
[6] G.B. Hoflund, D.F. Cox, R.E. Gilbert, J. Vac. Sci. Technol. A 1 (1983) 1837.
[7] Y. Nishino, A.R. Krauss, Y. Lin, D.M. Gruen, J. Nucl. Mater. 228 (1996) 346.
[8] D.A. Asbury, G.B. Hoflund, W.J. Peterson, R.E. Gilbert, R.A. Outlaw, Surf. Sci. 185 (1987) 213.
[9] B.J. Flinn, C.-S. Zhang, P.R. Norton, Phys. Rev. B 47 (1993) 16499.
[10] B. Li, K. Griffiths, C.-S. Zhang, P.R. Norton, Surf. Sci. 370 (1997) 97.
[11] C.-S. Zhang, B.J. Flinn, P.R. Norton, Surf. Sci. 264 (1992) 1.
[12] C.-S. Zhang, B.J. Flinn, I.V. Mitchell, P.R. Norton, Surf. Sci. 245 (1991) 373.
[13] Y.M. Wang, Y.S. Li, K.A.R. Mitchell, Surf. Sci. 342 (1995) 272.
[14] Y.M. Wang, Y.S. Li, K.A.R. Mitchell, Surf. Sci. 343 (1995) L1167.
[15] Y.M. Wang, Y.S. Li, K.A.R. Mitchell, Surf. Sci. 380 (1997) 540.
[16] P.C. Wong, K.A.R. Mitchell, Surf. Sci. 187 (1987) L599.
[17] W.T. Moore, P.R. Watson, D.C. Frost, K.A.R. Mitchell, J. Phys. C 12 (1979) L887.
[18] M. Yamamoto, C.T. Chan, K.M. Ho, S. Naito, Phys. Rev. B 54 (1996) 14111.
[19] B. Li, K. Griffiths, C.-S. Zhang, P.R. Norton, Surf. Sci. 384 (1997) 70.
[20] B. Li, A.R. Allnatt, C.-S. Zhang, P.R. Norton, Surf. Sci. 330 (1995) 276.
[21] C.-S. Zhang, B.J. Flinn, K. Griffiths, P.R. Norton, J. Vac. Sci. Technol. A 10 (1992) 2560.

[22] C.-S. Zhang, B.J. Flinn, P.R. Norton, J. Nucl. Mater. 199 (1993) 231.
[23] C.-S. Zhang, B. Li, P.R. Norton, J. Alloys Comp. 231 (1995) 354.
[24] J.T. Yates Jr., Methods of Experimental Physics, in: R.L. Park, M.G. Lagally (Eds.), Solid State Physics: Surfaces, vol. 22, Academic Press, Orlando, 1985.
[25] H.J. Kreuzer, Langmuir 8 (1992) 774.
[26] E.G. Seebauer, A.C.F. Kong, L.D. Schmidt, Surf. Sci. 193 (1988) 417.
[27] M. Kovar, K. Griffiths, R.V. Kasza, J.G. Shapter, P.R. Norton, V.P. Zhdanov, J. Chem. Phys. 106 (1997) 4797.
[28] B. Li, C.-S. Zhang, V.P. Zhdanov, P.R. Norton, Surf. Sci. 322 (1995) 373.